

Coding of repetitive transients by auditory cortex on posterolateral superior temporal gyrus in humans: an intracranial electrophysiology study

Kirill V. Nourski,¹ John F. Brugge,^{1,2} Richard A. Reale,^{1,2} Christopher K. Kovach,¹ Hiroyuki Oya,¹ Hiroto Kawasaki,¹ Rick L. Jenison,² and Matthew A. Howard III¹

¹Department of Neurosurgery, The University of Iowa, Iowa City, Iowa; and ²Department of Psychology, University of Wisconsin–Madison, Madison, Wisconsin

Submitted 16 August 2012; accepted in final form 11 December 2012

Nourski KV, Brugge JF, Reale RA, Kovach CK, Oya H, Kawasaki H, Jenison RL, Howard MA III. Coding of repetitive transients by auditory cortex on posterolateral superior temporal gyrus in humans: an intracranial electrophysiology study. *J Neurophysiol* 109: 1283–1295, 2013. First published December 12, 2012; doi:10.1152/jn.00718.2012.—Evidence regarding the functional subdivisions of human auditory cortex has been slow to converge on a definite model. In part, this reflects inadequacies of current understanding of how the cortex represents temporal information in acoustic signals. To address this, we investigated spatiotemporal properties of auditory responses in human posterolateral superior temporal (PLST) gyrus to acoustic click-train stimuli using intracranial recordings from neurosurgical patients. Subjects were patients undergoing chronic invasive monitoring for refractory epilepsy. The subjects listened passively to acoustic click-train stimuli of varying durations (160 or 1,000 ms) and rates (4–200 Hz), delivered diotically via insert earphones. Multicontact subdural grids placed over the perisylvian cortex recorded intracranial electrocorticographic responses from PLST and surrounding areas. Analyses focused on averaged evoked potentials (AEPs) and high gamma (70–150 Hz) event-related band power (ERBP). Responses to click trains featured prominent AEP waveforms and increases in ERBP. The magnitude of AEPs and ERBP typically increased with click rate. Superimposed on the AEPs were frequency-following responses (FFRs), most prominent at 50-Hz click rates but still detectable at stimulus rates up to 200 Hz. Loci with the largest high gamma responses on PLST were often different from those sites that exhibited the strongest FFRs. The data indicate that responses of non-core auditory cortex of PLST represent temporal stimulus features in multiple ways. These include an isomorphic representation of periodicity (as measured by the FFR), a representation based on increases in non-phase-locked activity (as measured by high gamma ERBP), and spatially distributed patterns of activity.

averaged evoked potential; click train; electrocorticography; high gamma; phase locking

ACOUSTIC TRANSIENTS ARE RICHLY represented in our environment, and the auditory system has evolved mechanisms for detecting these signals and encoding the information contained in them. These transients are brief signals, often referred to as “clicks”, and when they are repeated at equal intervals, the resulting percept is related to the rate at which they are presented. Clicks in a train presented at relatively low rates (<8–10 Hz) are perceived as individual events, whereas at progressively higher rates, the percept evolves into one of acoustic “flutter” and eventually (>30 Hz), one of pitch. In monkeys (Liang et al. 2002; Lu et al. 2001) and other mammals

(e.g., cats) (Imaizumi et al. 2010), neurons in the primary auditory cortex (A1) and immediately adjacent, primary-like fields (e.g., rostral and rostromedial in monkeys) use dual mechanisms to encode such acoustic transients: an isomorphic representation by precise timing of discharges at low repetition rates and a nonisomorphic (abstracted) representation by changes in overall firing rate at faster repetition rates (Wang 2007; Wang et al. 2003). Evidence from direct auditory cortical recording in humans suggests that similar mechanisms may be operating there as well (Brugge et al. 2009; Nourski and Brugge 2011).

In the classical sense, auditory cortex in humans, as in other primates studied so far, comprises multiple areas located on the superior temporal gyrus (STG) (Hackett 2011). The primary and primary-like cortex of the auditory core occupies the posteromedial aspect of Heschl’s gyrus (HG). This cortical complex is surrounded by multiple anatomically distinct auditory subdivisions on the anterolateral HG, planum polare, planum temporale, and lateral surface of the STG (Chiry et al. 2003; Hutsler and Gazzaniga 1996; Nakahara et al. 2000; Rivier and Clarke 1997; Wallace et al. 2002). Based largely on evidence derived from anatomical and physiological studies in monkeys, a functional model of the auditory cortex posits multiple fields interconnected in such a way as to provide for hierarchical processing of acoustic information (Hackett 2011; Kaas and Hackett 2005). This hierarchical model also provides a useful framework for investigating the functional organization of human auditory cortex (Rauschecker and Scott 2009). However, with the exception of the core cortex, the cross-species homologies of auditory cortical fields are still unclear [Fullerton and Pandya 2007; Hackett 2003, 2007, 2008, 2011; Hackett et al. 2001; Sweet et al. 2005; see Chevillet et al. (2011)].

Research performed in our laboratory uses direct intracranial recording in neurosurgical patients to study the functional organization of human auditory cortex. This method provides a unique opportunity to study multiple auditory cortical fields simultaneously and with high spatial and temporal resolution (Howard et al. 2012; Mukamel and Fried 2012). We have shown previously that local field potentials recorded from the posteromedial aspect of HG—the putative human homolog of the core field—exhibit robust temporal locking to click-train stimuli (Brugge et al. 2008, 2009). The response is characterized by large-amplitude, short-latency averaged evoked potentials (AEPs), increases in event-related band power (ERBP), and a frequency-following response (FFR). The phase-locked FFR is most prominent when elicited by click rates of ~50–

Address for reprint requests and other correspondence: K. V. Nourski, Dept. of Neurosurgery, The Univ. of Iowa, 200 Hawkins Dr., 1815 JCP, Iowa City, IA 52242 (e-mail: kirill-nourski@uiowa.edu).

100 Hz and below but may be detected reliably at rates as high as 200 Hz (Brugge et al. 2009). The morphology of the evoked waveforms and the range of phase locking are very similar to those response properties exhibited by the auditory core of macaque monkeys studied under similar stimulus conditions (Steinschneider et al. 1998).

In humans, processing of temporal information appears to engage non-core auditory fields as well as the auditory core (Giraud et al. 2000; Harms and Melcher 2002; Kuwada et al. 1986; Rees et al. 1986; Ross et al. 2000). An area adjacent to the putative core, on the anterolateral aspect of HG, has been shown to exhibit low-amplitude, long-latency AEPs and ERBP responses with the FFR weak or absent (Brugge et al. 2008, 2009; Liegeois-Chauvel et al. 1991). It was suggested that these recordings were obtained from one of the numerous putative auditory cortical belt areas in humans that have been identified anatomically. Previous work in our laboratory has also identified an acoustically responsive area on the posterior portion of the lateral STG, functionally distinct from auditory areas on HG. We refer to this area as the posterolateral superior temporal (PLST) auditory area (Howard et al. 2000). This area, which may comprise more than one functional field, was found to respond robustly to a wide range of stimuli, from tone and noise bursts to speech utterances (Brugge et al. 2008; Howard et al. 2000; Steinschneider et al. 2011), the latter influenced by the visual presentation of congruent face and lip movements (Reale et al. 2007). Electrical stimulation tract-tracing studies further revealed a short-latency functional connection between PLST and the auditory core on HG (Brugge et al. 2003, 2005).

We also noted that certain sites in PLST exhibited robust phase locking to clicks and have presented some of these results in abstract form (Nourski et al. 2011). Accordingly, we hypothesized that non-core auditory fields on the lateral STG would, like the auditory core, also exhibit isomorphic and nonisomorphic representations of temporal acoustic events, albeit on different time scales. Here, we present details of these studies, comparing response dynamics observed within PLST with those exhibited by the auditory core and characterizing their spatial distribution. In doing so, we provide a framework for future studies aimed at establishing the role of explicit cortical representation of temporal information in the higher functions of speech perception and comprehension.

METHODS

Subjects. Experimental subjects were 16 neurosurgical patients (10 male, six female, age 20–56 yr, median age 34.5 yr). The subjects had been diagnosed with medically refractory epilepsy and were undergoing chronic invasive electrocorticogram (ECoG) monitoring to identify seizure foci prior to resection surgery. Written, informed consent was obtained from each subject. Research protocols were approved by The University of Iowa Institutional Review Board.

Thirteen subjects reported themselves to be right-handed, two (L147 and R180) to be left-handed, and one (L151) to be ambidextrous. All subjects but one had left-hemisphere language dominance, as determined by intracarotid amyltal (Wada) test results; subject L162 had bilateral language representation. The placement of the electrode arrays was based on clinical considerations, and for that reason, we were unable to record from both the left and right hemisphere in the same subject. In seven subjects, the electrodes were implanted on the left side, whereas in nine others, the recordings were obtained from the right hemisphere. The side of implantation is indicated by the letter prefix of the subject code (L for left; R for right). All subjects

underwent audiometric and neuropsychological evaluation before the study, and none was found to have hearing or cognitive deficits that might impact the findings presented in this study. All subjects were native English-language speakers. Clinical analysis of intracranial recordings indicated that the auditory cortical areas on the STG were not involved in generation of epileptic activity in any of the subjects included in this study.

Each subject underwent whole-brain, high-resolution, T1-weighted, structural MRI (resolution 0.78×0.78 mm, slice thickness 1.0 mm, average of two) scans, before and after electrode implantation, to determine recording contact locations relative to the preoperative brain images. Preimplantation MRIs and postimplantation, thin-sliced volumetric computed tomography (CT) scans (in-plane resolution 0.51×0.51 mm, slice thickness 1.0 mm) were coregistered using a three-dimensional (3D) linear registration algorithm (Functional MRI of the Brain Linear Image Registration Tool) (Jenkinson et al. 2002). Coordinates for each electrode contact obtained from postimplantation CT volumes were transferred to preimplantation MRI volumes. Results were compared with intraoperative photographs to ensure reconstruction accuracy.

Experiments were performed in a dedicated electrically shielded suite located within the Clinical Research Unit of the University of Iowa Institute for Clinical and Translational Science. The subjects were reclining in a hospital bed or an armchair and were awake but not actively attending to the stimuli.

Stimuli. Experimental stimuli were trains of acoustic clicks, digitally generated as equally spaced rectangular pulses (0.2-ms duration) and delivered to both ears via insert earphones (ER4B; Etymotic Research, Elk Grove Village, IL) that were integrated into custom-fit earmolds. The stimuli were presented at a comfortable level, typically ~50 dB above hearing threshold.

Two stimulus configurations were used: short-duration (160-ms) click trains of 25, 50, 100, 125, 150, and 200 Hz and long-duration (1-s) click trains of 4, 8, 16, 32, 64, and 128 Hz. In seven early experiments (R127, R129, L130, L138, R139, L140, and R142), each stimulus of a particular click rate was presented 100 times, after which, the next click rate was chosen and the procedure repeated until stimulus sets representing the six different click rates had been delivered. In later experiments (L147, L151, R152, R153, R154, L162, L178, R180, and R186), click-train stimuli of the six rates were each presented 50 times in random order. In all experiments, the intertrain interval was chosen randomly within a Gaussian distribution (mean interval 2 s; SD = 10 ms) to reduce stimulus predictability and to allow more efficient AEP estimation. Stimulus delivery and data acquisition were controlled by a RP2.1 and RX5 or RZ2 real-time processor (Tucker-Davis Technologies, Alachua, FL).

Recording. Details of electrode implantation and data collection have been described previously (Brugge et al. 2008; Howard et al. 2000, 2012). In brief, filtered (1.6- to 1,000-Hz bandpass, 12-dB/octave rolloff) and amplified (20 \times) ECoG data were digitally recorded (sampling rate 2,034.5 Hz) from multicontact, subdural grid electrodes (Ad-Tech Medical Instrument, Racine, WI) placed over the perisylvian cortex, including the STG. The recording arrays consisted of 96 platinum-iridium disc electrodes (2.3-mm exposed diameter, 5-mm interelectrode distance) arranged in an 8×12 grid and embedded in a silicon membrane. A subgaleal contact was used as a reference. Simultaneous recordings were obtained from hybrid-depth electrodes, stereotactically implanted into the HG, roughly parallel to its long axis (Howard et al. 1996; Reddy et al. 2010). Data obtained from those recordings have been reported in detail previously (Brugge et al. 2009). Recording electrodes remained in place up to 2 wk under the direction of clinical epileptologists.

Analysis. ECoG data obtained from each recording site was analyzed as the AEP and in the time-frequency plane, as ERBP. Data analysis was performed using custom software, written in a MATLAB Version 7.13.0 programming environment (MathWorks, Natick, MA). Preprocessing of ECoG data included downsampling to 1 kHz, fol-

lowed by removal of power-line noise by an adaptive notch-filtering procedure. To identify peaks in the power spectrum associated with line noise, the log Fourier power spectrum was normalized by a smoothed baseline value. The baseline was obtained from the interpolation of an eighth-order polynomial, fitted to the log spectrum by least squares. Peaks in the baseline-normalized signal were extracted using a threshold criterion. For each fundamental frequency among extracted peaks, the entire data sequence was divided into overlapping windows of ~ 4 -s length adjusted to match, as nearly as possible, an integer multiple of the fundamental period. The purpose of the latter step is to minimize spectral leakage from peaks at the targeted line noise frequency. Fourier components at the fundamental and harmonic frequencies were then removed from the data within the overlapping windows. De-noised data were reconstructed by applying a weighted average, w , between overlapping windows, where the k^{th} point in the window was weighted by

$$w[k] = \frac{1 - \cos\left(\frac{2\pi k}{N}\right)}{2}$$

where N is the window length.

Additionally, single-trial (peristimulus) ECoG waveforms with voltage peaks or troughs >2.5 SD from the mean were eliminated from the data set prior to further analyses. This would include sporadic activity generated by electrical interference; epileptiform spikes; high-amplitude, slow-wave activity; or movement artifacts.

Single-trial waveforms, obtained on the 96 cortical sites, were transformed at every time point with a spatial filter using the surface Laplacian operation (Nunez 1981; Nunez and Pilgreen 1991; Reale et al. 2007). The surface Laplacian is independent of the reference electrode and reduces the effects of spatial smearing of ECoG voltage due to volume conduction in the tissue and fluid of the brain. The surface Laplacian required an accurate representation of the spatial distribution of potential, which was estimated using a 2D thin-plate spline interpolant with clamped edges (Law et al. 1993; Perrin et al. 1987). We have shown previously that this procedure yields a noticeable increase in the spatial specificity of the recordings from PLST compared with unprocessed data (Reale et al. 2007).

The magnitude of the AEP was characterized by the root mean square (RMS) amplitudes within the time interval of 300 ms after stimulus onset. Phase-locked responses to the periodicity of the click trains were visualized as the FFR by high-pass filtering AEP waveforms with a cutoff of one octave below the driving frequency using a fourth-order Butterworth filter (24-dB/octave slope with zero-phase shift). FFRs were quantified using the phase-locking value (PLV) metric (Jervis et al. 1983), calculated from single-trial ECoG signals within a window of 50–250 ms after stimulus onset, tapered with a Tukey function. The PLV is an amplitude-independent metric of response synchrony and thus has the potential for accurate separation of phase-locked response components from non-phase-locked activity (Chavez et al. 2006). PLVs are often computed in the time domain using bandpass-filtered and Hilbert-transformed analytic signals (Lachaux et al. 1999). We computed PLVs in the frequency domain using the FFT of the 200-ms window. Significance of PLVs was evaluated by applying the likelihood ratio test (Pawitan 2001) to numerically evaluated maximum-likelihood fits of a von Mises distribution, wherein the null hypothesis had a uniform distribution of phase angles over trials. This procedure is equivalent to the Rayleigh test (Mardia and Jupp 2000). Correction for multiple comparisons was done by controlling false discovery rate (Benjamini et al. 2001; Benjamini and Hochberg 1995) at $q = 0.01$. Phase locking to 25 Hz often failed to reach statistical significance in our data sets. This negative finding can be attributed to the number of clicks (five) in the train in this stimulus condition, which may have been too small to allow a measurable FFR to develop. In addition, the FFR at 25 Hz was sometimes difficult to separate from the onset AEP waveform, as their

time course and dominant spectral features overlapped. As a result, significant PLVs at frequencies close to 25 Hz were sometimes observed in the absence of a 25-Hz driving stimulus.

Time-frequency analysis of the ECoG was performed using wavelet transforms based on complex Morlet wavelets following the approach of Oya et al. (2002). Center frequencies ranged from 20 to 200 Hz in 5-Hz increments. ERBP was calculated for each center frequency on a trial-by-trial basis and normalized to median baseline power, measured for the same center frequency within a 100- to 200-ms window prior to stimulus onset. ERBP values were then log-transformed and averaged across trials. For quantitative analysis of ERBP, we focused on the high gamma ECoG frequency band (Brugge et al. 2009; Crone et al. 2001; Edwards et al. 2009), which was defined in the present study within a range of center frequencies between 70 and 150 Hz. The wavelet constant ratio used for time-frequency analysis was defined as $f_o/\sigma_f = 9$, where f_o is the center frequency of the wavelet, and σ_f is its SD in the frequency domain. At this wavelet constant value, contribution of energy from the post-stimulus onset interval to the estimate of baseline power is negligible for the range of center frequencies that correspond to the high gamma frequency band (Steinschneider et al. 2011). The magnitude of high gamma ERBP was taken as the average power within the 50- to 250-ms time window after stimulus onset. Maps of AEP and ERBP cortical activation were smoothed using triangle-based cubic interpolation with an up-sampling factor of 16 for display purposes.

For statistical analyses, we used the ANOVA model that is commonly used to test hypotheses concerning the effects of experimental factors on a dependent, univariate response measurement (e.g., either ERBP or PLV). One set of observations consisted of ERBP or PLV measurements, obtained at unique recording sites, located in either left- or right-hemisphere locations for each tested click rate. Thus for this response metric, we had one repeated-measures, within-subjects factor ("click rate" with six levels for ERBP: 25, 50, 100, 125, 150, and 200, or five levels for PLV: 50, 100, 125, 150, and 200) and one between-subjects factor ("laterality" with two levels: left and right). We emphasize that members of our sample are unique "recording site locations", although referred to here in the standard statistical parlance as subjects. A second sample of observations consisted of ERBP or PLV measurements for each of five click rates obtained at a unique recording site located on PLST and at a site in medial HG located in the same hemisphere. Thus for this design, we had one repeated-measures, within-subjects factor (click rate with five levels: 50, 100, 125, 150, 200) and one between-subjects factor ("location" with two levels: PLST and medial HG).

We used a generalized linear model (GLM) approach (SAS 9.3 Procedure GLM; SAS Institute, Cary, NC) to these repeated-measures ANOVAs, because it did not require the assumption of sphericity and could accommodate unequal sample sizes. The SAS GLM procedure for repeated measures for a one-dependent variable response produced two different sets of the within-subjects hypothesis tests: one using the multivariate approach and the other using the univariate approach. Generally, both sets of tests yielded similar results. The multivariate measures that provided for testing effects, as well as for any specified contrast (e.g., testing for a linear trend), included Wilks' lambda, Pillai's trace, Hotelling-Lawley trace, and Roy's greatest root. We report results using only Pillai's trace, because it is considered more robust to violations of the multivariate's assumption of homogeneity of variance/covariance matrices. Nevertheless, almost identical conclusions were reached using any of the above measures.

Spatial relationship between high gamma activity and FFRs was measured in each subject using Pearson's correlation between averaged high gamma ERBP and PLVs measured in individual recording channels, followed by a repeated-measures ANOVA on Pearson's R values.

Modulation of high gamma ERBP by the stimulus temporal envelope was evaluated for long (1-s) click-train stimuli, presented at relatively low rates (4, 8, and 16 Hz). By analogy with FFR measure-

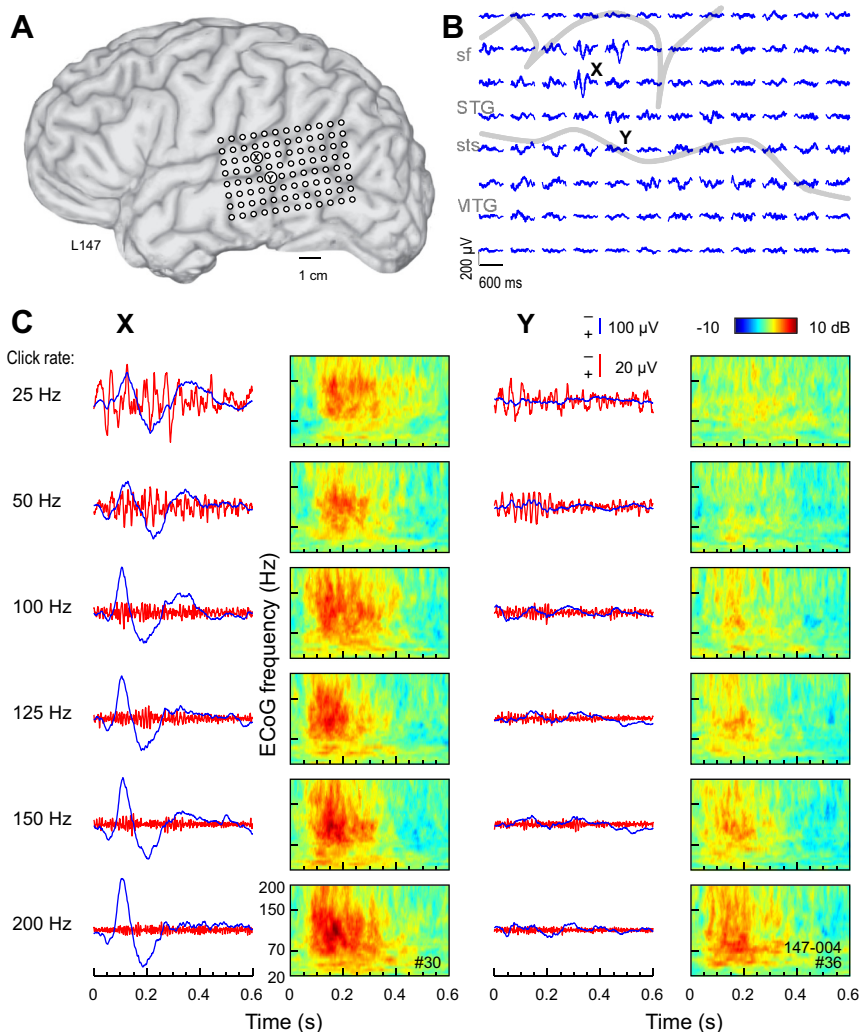


Fig. 1. Auditory cortical responses to click-train stimuli recorded from the left hemisphere in a representative subject. *A*: location of the 96-contact subdural grid. *B*: all-pass (1.6- to 500-Hz bandpass) averaged evoked potential (AEP) waveforms recorded from the subdural grid in response to 160-ms, 100-Hz click trains. Negative voltage is plotted upward. Sulcal patterns are indicated by gray outlines. MTG, middle temporal gyrus; sf, sylvian fissure; STG, superior temporal gyrus; sts, superior temporal sulcus. *C*: All-pass (1.6–500 Hz) and high-pass (cut-off 1 octave below driving frequency) AEP waveforms (blue and red traces, respectively) and time-frequency analysis of electrocorticogram (ECoG; color plots) recorded in response to click trains presented at rates between 25 and 200 Hz (*top to bottom*). Data from 2 recording sites, indicated by X (at which the AEP of greatest amplitude was recorded) and Y (that was some distance away, and where the AEP was of lower amplitude), are shown.

ments, PLVs were calculated from single-trial, high gamma ERBP signals within a window of 250–1,000 ms after stimulus onset. Significance of PLVs, representing modulation of high gamma ERBP by the driving frequency of the click-train stimuli, was assessed with correction for multiple comparisons (false discovery rate, $q = 0.01$).

RESULTS

Series 1: short click trains. The cardinal features of responses (AEP, FFR, and ERBP) recorded from sites on STG of the left hemisphere of one subject (Fig. 1) and the right hemisphere of another (Fig. 2) are presented. In each case, click-train stimulation elicited robust responses characterized by AEP waveforms and their spatial distributions consistent with those described for PLST in our earlier reports (Howard et al. 2000; Reale et al. 2007). Each AEP map shown in Figs. 1*B* and 2*B* marks the recording site at which the AEP of greatest amplitude was recorded, as well as a second site within PLST that was some distance away and where the AEP was of lower amplitude. The AEP, FFR, and ERBP derived from responses at these two sites to click trains of increasing rates are shown overlapped in Figs. 1*C* and 2*C*. The AEP and ERBP exhibited an increase and the FFR, a decrease in magnitude with increase in click rate. The increase in magnitude of the AEP and ERBP was accompanied by a decrease in response

latency. The growth in magnitude of the ERBP occurred across a wide range of ECoG frequencies, from ~ 30 Hz to at least 200 Hz. As a rule, the largest ERBP responses were observed between ~ 100 ms and ~ 300 ms after stimulus onset. Hence, at any click rate, ERBP temporally overlapped the AEP and FFR but exhibited a longer latency.

Statistical analysis of the ERBP sample population indicated that the assumption of sphericity was violated (Mauchly's sphericity test), $\chi^2(14) = 668.839$, $P < 0.0001$. Consequently, degrees of freedom were adjusted using the Greenhouse-Geisser correction. Subsequent analyses revealed that click rate had a significant main effect [$F(2.96, 1,412) = 238.02$, $P < 0.0001$] and that ERBP values tended to increase linearly (using Pillai's trace statistic) with click rate [$F(1, 477) = 494.10$, $P < 0.0001$]. Mean ERBP values for left-hemisphere cases were observed to be lower than for right-hemisphere cases, as supported by a significant main effect [$F(1, 477) = 9.52$, $P < 0.005$] for laterality. Subsequent post hoc *t*-tests (Tukey-Kramer adjustment for multiple comparisons: $P < 0.05$) indicated lower left-hemisphere ERBP values at all six click rates. There was no significant interaction between click rate and location factors [$F(2.96, 1,412) = 2.47$, $P = 0.0785$].

FFR strength was quantified in terms of PLVs. Figure 3 shows PLVs as functions of click rates for all recording sites in

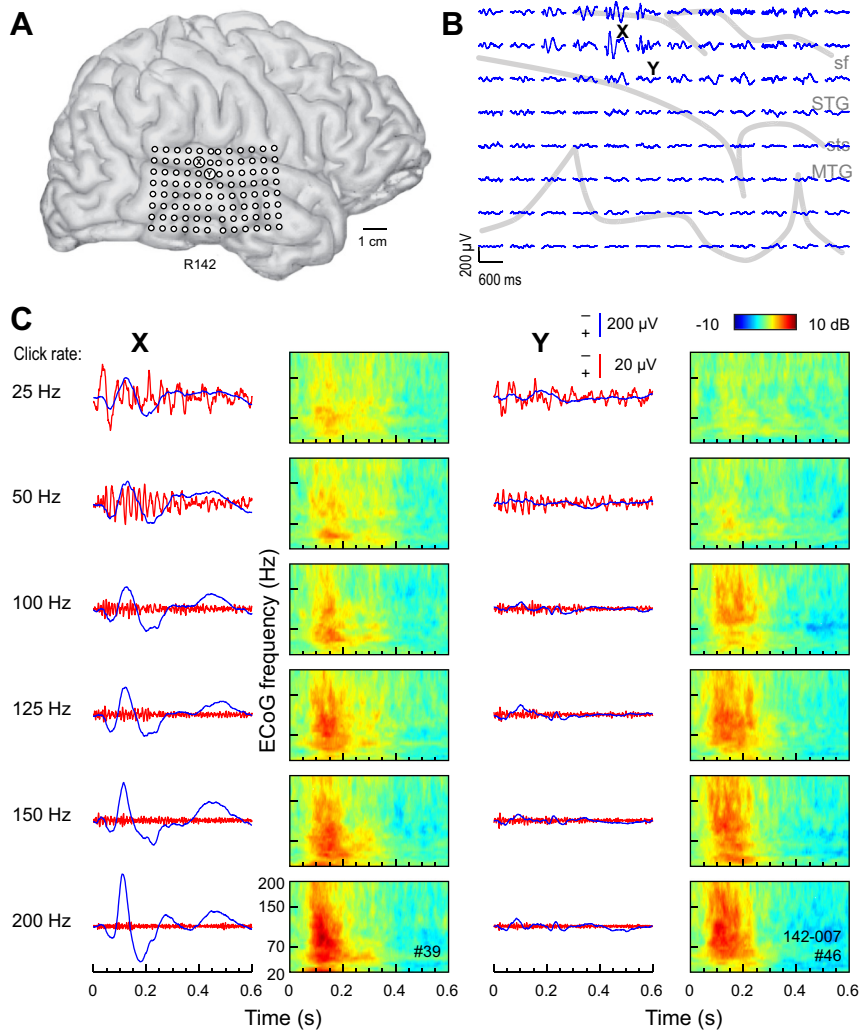


Fig. 2. Auditory cortical responses to click-train stimuli recorded from the right hemisphere in a representative subject. See legend of Fig. 1 for details.

all subjects that exhibited a significant ($q < 0.01$) PLV to at least one of the five stimuli (50, 100, 125, 150, and 200 Hz). The FFR was typically most prominent at 50 Hz, with its amplitude dropping off above that rate. The total number of recording sites across the 14 subjects that exhibited significant PLVs to 50-, 100-, 125-, 150-, and 200-Hz click trains was 153, 16, 7, 9, and 3, respectively. Phase locking to 25 Hz often failed to reach significance for reasons explained in METHODS, and hence, the 25-Hz stimulus condition was excluded from quantitative analyses of responses to the short click-train series.

To better fit the assumptions of normality and homogeneity of variances, PLV data were transformed (arcsin of square root) prior to parametric statistical procedures. Transformed variables did not violate the assumption of sphericity (Mauchly's sphericity test), $\chi^2(9) = 15.37$, $P = 0.08$. The resulting analysis revealed that click rate had a significant main effect [$F(4, 488) = 124.70$, $P < 0.0001$], whereas the influence of laterality was nonsignificant [$F(1, 122) = 1.74$, $P = 0.1895$]. Thus there was no significant difference between PLVs in left- and right-hemisphere sites. Both multivariate [$F(4, 119) = 2.98$, $P = 0.0218$] and univariate [$F(4, 448) = 2.73$, $P = 0.0287$] tests indicated a significant interaction effect of click rate by laterality on PLVs. However, the interaction between

these two variables may be too small to have any practical significance, since the main effect for click rate was much stronger than that for this interaction.

Functional maps. Spatial maps of AEP, FFR, and ERBP were derived from responses to click trains of different rates from all 16 subjects in the study. Although the maps derived from the three measures overlapped, they were not coextensive. The AEP, FFR, and ERBP were not always maximal at the same locations, and at any given cortical site, they were often present in varying degrees. The spatial distribution of cortical responses to click trains presented at different stimulus rates is shown for two representative left-hemisphere (Fig. 4, A and B) and two right-hemisphere cases (Fig. 5, A and B). The map shown in Fig. 4A is derived from the data shown in Fig. 1A, and the one shown in Fig. 5A is derived from data shown in Fig. 2A. Data are plotted as interpolated cortical activation maps, showing both the distribution of normalized RMS magnitude of the AEP and of high gamma ERBP. The contour patterns associated with AEPs and ERBP were rather complex and often characterized by the presence of multiple active foci that changed shape and grew in size with changes in click rate. There was no consistent evidence of an orderly representation of cortical sites preferentially responding to specific driving frequencies. Whereas there was a certain consistency in the

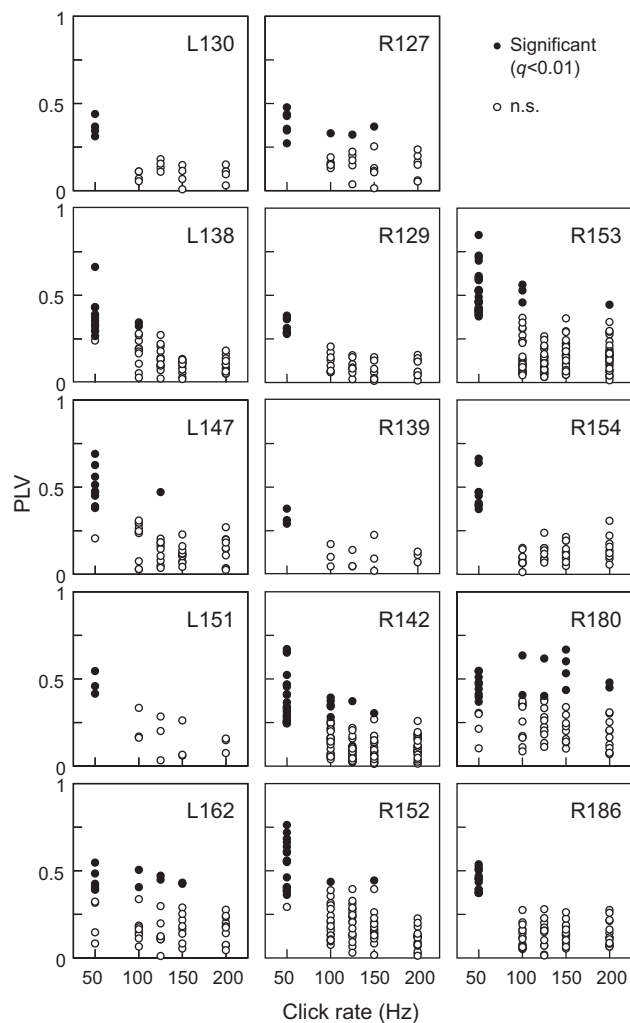


Fig. 3. Phase locking to click trains recorded from 14 subjects. Phase-locking values (PLVs) are plotted as functions of click rate. In each subject, data from sites that exhibited significant phase locking ($q < 0.01$) to at least 1 stimulus rate out of 5 are shown.

spatial distribution of AEPs with patterns of high gamma activity in individual subjects, the two response features were not entirely congruent.

The extent of spatial overlap between high gamma ERBP and phase-locked responses (PLVs) was quantified for each subject using Pearson's correlation. Repeated-measures ANOVA on Pearson's R values revealed a significant effect of frequency [$F(4, 56) = 12.8, P < 0.0005$]. A significant linear trend [$F(1, 14) = 47.9, P < 0.0005$] indicated that the two features of the cortical response—high gamma ERBP and the FFR—were more spatially congruent at lower click rates (Fig. 6). Furthermore, repeated-measures ANOVA revealed a significant between-subjects effect of laterality [$F(1, 14) = 8.96, P < 0.02$], with left-hemisphere data characterized by lower Pearson's R values. There was no significant laterality–frequency interaction [$F(4, 56) = 1.23, P = 0.361$]. Thus there was a greater spatial disconnect between ERBP responses and PLV in the left-hemisphere cases compared with the right-hemisphere subjects. Specifically, cortical sites that exhibited significant FFRs to the driving frequency (Figs. 4 and 5) were often located just

outside regions where AEPs and ERBP were of greatest magnitude.

Relationship to responses obtained simultaneously on HG. A majority of the subjects in this study were also implanted with multicontact depth electrodes in the superior temporal plane that targeted auditory cortex on HG. Thus it was possible to record simultaneously click-elicited activity across a range of click rates from the lateral surface of the temporal lobe, including PLST, as well as presumed auditory core cortex and adjacent non-core fields in HG. An example of such a comparison is shown in Fig. 7. Responses to click trains presented at rates between 25 and 200 Hz are shown for three cortical sites (Fig. 7A): a representative PLST site, a presumed core cortex site in medial HG, and a site in a nonprimary field on lateral HG. Consistently with our previous studies (Brugge et al. 2008, 2009; Howard et al. 2000), AEP waveforms recorded in response to click trains had a different morphology among the three different locations (Fig. 7B). AEPs recorded from PLST often (but not always) had smaller amplitudes than those recorded from medial HG yet were typically larger and had shorter latencies than AEPs recorded from lateral HG. Comparison of FFRs revealed across-field differences in capacity for synchronization to the stimulus periodicity. PLST reliably exhibited FFRs to click trains presented at 50–100 Hz and rarely to higher rates (see Fig. 3), whereas medial HG could typically phase lock to 200-Hz click trains [see Brugge et al. (2009)].

PLVs that characterized synchronization to the stimulus periodicity were consistently higher for medial HG sites compared with PLST (Fig. 8). For statistical analysis of this observation, the sample of PLV observations was constructed by choosing those medial HG sites for which there were also simultaneously recorded PLST sites in the same hemisphere. Only those PLST electrode sites that evidenced the largest PLV values in response to 50-Hz click trains in each tested subject were included. The assumption of sphericity could not be rejected in this sample [Mauchly's sphericity test: $\chi^2(9) = 12.294, P = 0.1972$], and inferences from multivariate and univariate tests agreed. The resulting analysis revealed that the click rate had a significant main effect [$F(4, 64) = 34.69, P < 0.0001$] on transformed PLVs. This influence was also dependent on location [medial HG vs. PLST; $F(1, 19) = 19.05, P < 0.0005$]. Subsequent post hoc t -tests (Tukey-Kramer adjustment for multiple comparisons: $P < 0.02$) indicated that PLVs in PLST were consistently lower than medial HG values for all five studied click rates. The interaction between click rate and recording location was not significant [$F(4, 64) = 1.54, P = 0.2020$].

Lateral HG only occasionally exhibited a FFR, which was considerably weaker than that in PLST and if at all present, was limited to relatively low stimulus rates (25–50 Hz). Finally, ERBP analysis revealed differences in magnitude and latency of ECoG power changes among the three sampled cortical areas (see Fig. 7B). Putative core auditory cortex of medial HG had consistently shorter latency of ERBP changes compared with PLST and lateral HG. At low rates (e.g., 25 Hz), activity recorded from medial HG featured bursts of high gamma ERBP that were temporally related to the FFR and followed each successive click in the train. Such bursts or modulation of high gamma ERBP at low stimulus rates were not present in recordings made from either PLST or lateral HG.

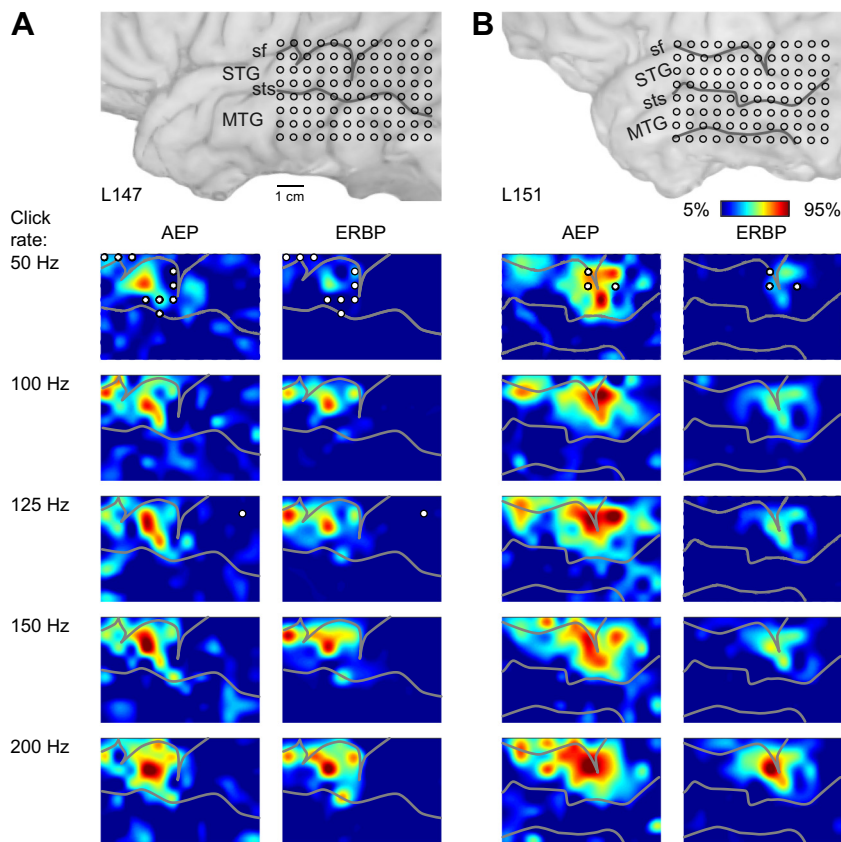


Fig. 4. Spatial distribution of cortical responses to click trains recorded from the left hemisphere in 2 representative subjects (shown in *A* and *B*). In each panel, location of the recording grid is shown on the *top*, followed by cortical activation maps across click rates (*top-to-bottom* rows), as measured by AEP root mean square (RMS) amplitude and high gamma event-related band power (ERBP; *left* and *right* columns, respectively). AEP RMS amplitudes were calculated within 0–300 ms after stimulus onset; high gamma ERBP was averaged within 50–250 ms after stimulus onset for each recording site, normalized relative to the maximum values across stimuli in each subject and smoothed using cubic interpolation. Sulcal patterns are shown by gray lines. Circles indicate sites that exhibited significant (at $q = 0.01$) PLVs at each stimulus rate.

Series 2: long (1-s) click trains. Results presented in Figs. 1–7 were obtained using relatively short-duration (160-ms) click-train stimuli, delivered at rates between 25 and 200 Hz. In a subset of subjects ($n = 6$), we used a complementary set of longer-duration (1-s) click trains, which were presented at a different range of repetition rates (4–128 Hz). Although these stimuli were not studied as extensively as the short-duration click trains, Fig. 9 presents examples of responses to these stimuli recorded from representative PLST sites in two different subjects (Fig. 9, *A* and *C*, and Fig. 9, *B* and *D*, respectively). At a relatively low rate of 4 Hz, each click in the train evoked a distinct AEP complex (Fig. 9, *A* and *B*). Here, the interclick interval of 250 ms was long enough for each AEP to develop to each individual click in the train. This is illustrated further in Fig. 9, *C* and *D*, which depicts portions of the AEP waveforms that correspond to responses elicited by individual clicks. Early components of the AEP waveform that were associated with each click in the train resembled the morphology of onset of the AEP complex in response to a higher-rate (128-Hz) stimulus. As the rate increased to 8–16 Hz, responses to successive clicks overlapped, and as the click rate increased beyond 16 Hz, distinct on- and off-response AEP complexes emerged. Activity within PLST—elicited by click trains presented at rates up to at least 64 Hz—contained a FFR component, which was particularly noticeable in the AEP waveform at 16- to 32-Hz stimulus rates.

Time-frequency analysis of ECoG revealed patterns of high gamma ERBP responses to click trains within PLST. At low repetition rates (4–16 Hz), click trains elicited very modest changes in high gamma power. High gamma ERBP typically was not modulated by the stimulus envelope of the click trains

presented at 4–16 Hz. PLV analysis failed to reveal significant (at $q = 0.01$) modulation of high gamma ERBP by the driving frequency of click trains presented at these repetition rates in any PLST recording site in five out of six subjects tested using this paradigm. In the remaining subject (R152), significant PLVs characterized responses obtained from three recording sites located on the STG.

As stimulus rate increased, stronger ERBP responses emerged, peaking at ~100–150 ms after stimulus onset and then decreasing gradually over the duration of the 1-s-long train. Overall, results obtained from experiments with 1-s click trains paralleled our findings with the 160-ms click-train series. In both sets of experiments, we observed a dual representation of repetitive stimuli by synchronized and non-phase-locked high gamma cortical activity at low and high repetition rates, respectively.

DISCUSSION

There were three major findings related to the complex temporal and spatial patterns elicited in PLST by click trains of varying rates. First, the AEP was synchronized to individual clicks in the train for click rates below ~150–200 Hz. Phase locking to clicks tended to be maximal ~50 Hz and decline systematically with increasing click rate. Decline in phase locking was associated with an increase in the amplitude of the AEP. At any given click rate, between 50 and 200 Hz, phase locking tended to be weaker in PLST than in the putative auditory core cortex. The AEP is interpreted to represent the incoming volley of afferent activity and subsequent synaptic currents (Steinschneider et al. 1992, 1994; Vaughan 1969; Vaughan and Arezzo 1988). Second, the dis-

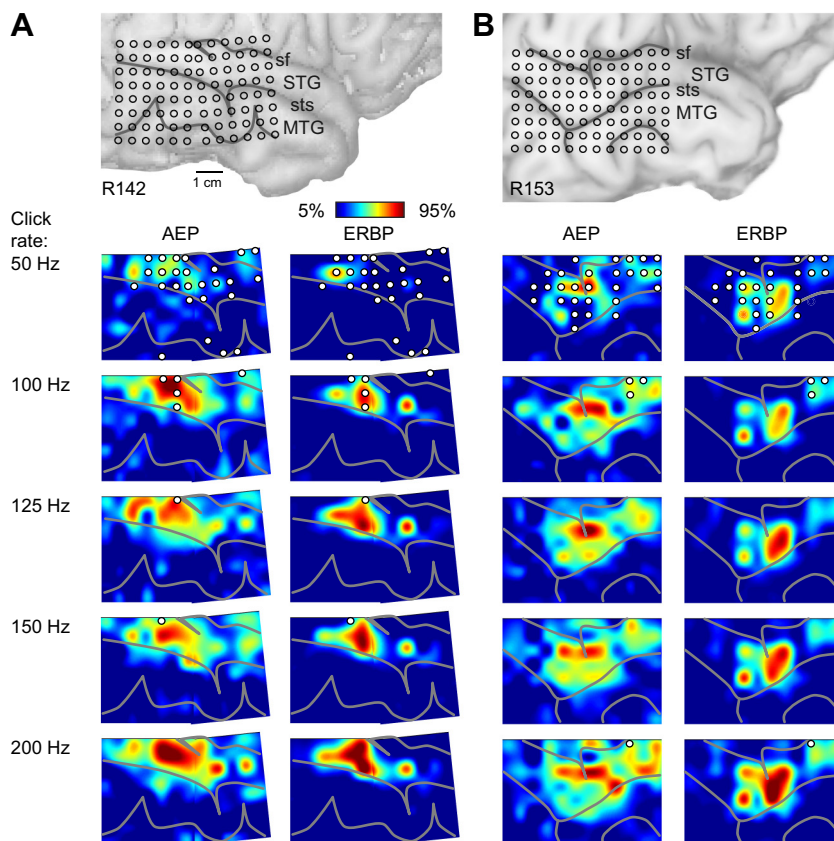


Fig. 5. Spatial distribution of cortical responses to click trains recorded from the right hemisphere in 2 representative subjects (shown in A and B). See legend of Fig. 4 for details.

tributions within PLST of phase-locked AEP and of ERBP were overlapping but not coextensive. Third, cortical activity in PLST in the high gamma frequencies, unlike that of the auditory core, was not temporally modulated by individual clicks when the click trains were presented at relatively low rates (<30 Hz; i.e., below the lower limit of pitch) (Krubmholz et al. 2000). Like the AEP, however, the magnitude of the

ERBP generally increased with click rate. ECoG frequencies within the high gamma band have been shown to be associated with both spiking activity and hemodynamic changes (Nir et al. 2007; Whittingstall and Logothetis 2009), which allows direct comparison of data obtained under different experimental conditions.

Phase-locked responses to click trains. Temporal representation of stimulus periodicity is a basic property of the auditory system found on all levels from the auditory nerve to the auditory cortex (Joris et al. 2004; Langner 1992). At the cortical level, direct electrophysiological study of temporal processing has been largely confined to the auditory core of awake monkeys listening to sinusoidally amplitude-modulated (SAM) sounds [reviewed by Wang (2007) and Wang et al. (2003)]. In humans, Liégeois-Chauvel et al. (2004) measured phase locking to SAM noise bursts by calculating the power of the AEP signal at the driving modulation frequency. For core cortex, the strongest phase locking was most often found at 8 Hz but could be seen as high as 32 Hz, whereas for lateral STG, the best modulation frequency did not exceed 16 Hz. Direct comparison of findings reported by Liégeois-Chauvel et al. (2004), using AEP power with the data presented in our study, is not appropriate, because we used a power-independent metric (PLV) to characterize cortical phase-locked activity.

Ongoing cortical activity is known to exhibit the inverse power law behavior, with log power decreasing nearly linearly with increasing log frequency (Buszaki 2006). Therefore, power in the spectra of the AEP can be expected to decrease with frequency regardless of whether a FFR is actually present or not. In a study that investigated auditory cortical responses to bursts of SAM noise, Gourévitch et al. (2008) corrected for

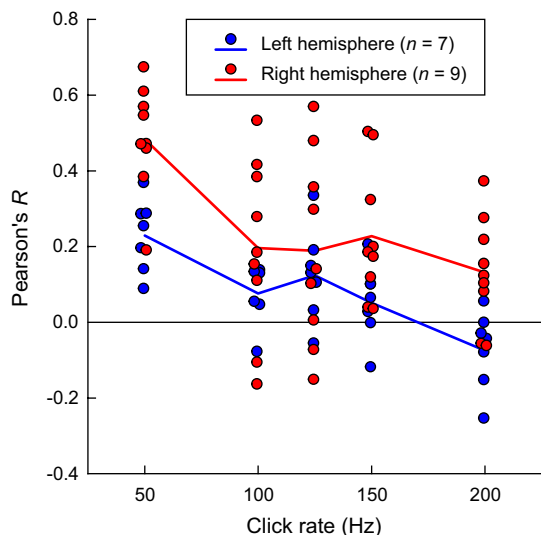


Fig. 6. Correlation between high gamma ERRP and PLV at different click rates. Data from 96 contact subdural grids implanted in the left hemisphere in 7 subjects (blue circles) and in the right hemisphere in 9 other subjects (red circles). Blue and red lines represent mean Pearson's *R* values for left- and right-hemisphere cases, respectively. A small amount of variability was added to the abscissa values to make individual data points more visible.

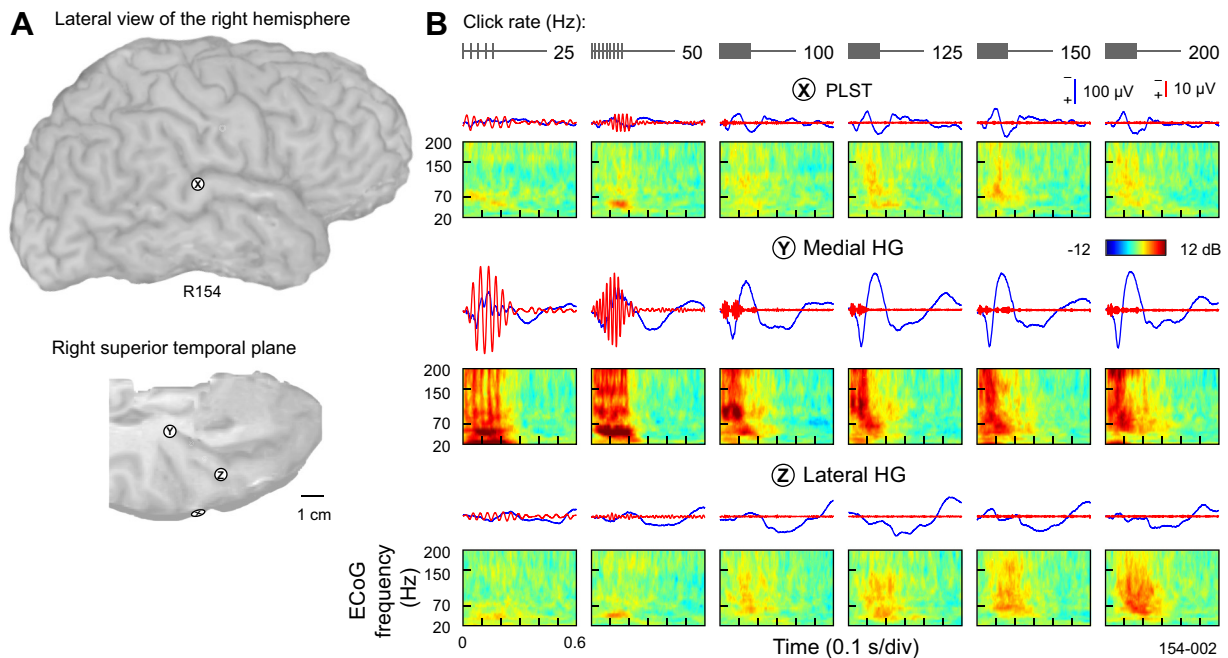


Fig. 7. Comparison of responses to click trains between PLST and 2 recording locations within Heschl's gyrus (HG). *A*: location of 3 exemplary recording sites—a representative PLST site, a presumed core cortex site in medial HG, and a site in a nonprimary field on lateral HG (marked by X, Y, and Z, respectively) in a representative subject. *B*: AEPs, FFRs, and ERBP obtained from PLST, core auditory cortex in medial HG, and a non-core field in lateral HG (top to bottom). Stimuli: 160-ms click trains, presented at rates between 25 and 200 Hz (left to right). Stimulus schematics are shown in top rows.

the $1/f$ ECoG characteristic and estimated the strength of the FFRs as a signal-to-noise ratio. In their study, the power of the AEP signal at the driving frequency was normalized to an estimate of background activity power at the same frequency. Responses recorded from sites on the lateral STG were characterized by lower signal-to-noise ratios compared with those recorded from HG across a range of modulation frequencies between 4 Hz and 128 Hz. Nevertheless, several sites on the

lateral STG were shown to exhibit signal-to-noise ratios between 10 dB and 15 dB at 64-Hz stimulation and between 5 dB and 10 dB in response to a 128-Hz amplitude-modulated noise stimulus (Gourévitch et al. 2008). These observations are consistent with our present findings.

As shown in the present study (see Figs. 1C, 2C, and 9, A and B) and elsewhere (Brugge et al. 2009; Nourski and Brugge 2011), cortical responses to repetitive stimuli, presented at rates above ~ 30 Hz, are characterized by increases in cortical activity in gamma and high gamma ECoG frequency bands. This constitutes a potential confounding factor for estimation of the FFR from the AEP power spectra to repetition rates that correspond to the frequency range of the non-phase-locked ERBP response. AEPs are typically averaged over a relatively small number of trials (50–100 in this study). Time-domain averaging of peristimulus epochs minimizes the contribution of non-phase-locked components to the AEP but does not eliminate it completely. Therefore, the power spectrum of the AEP may feature a power increase resulting from residual (uncanceled by time-domain averaging), non-phase-locked activity in gamma and high gamma bands, overlapping with the driving frequency. Such circumstances may lead to a false-positive detection of the FFR if it is estimated from this AEP power spectrum.

This reasoning motivated us to take advantage of the PLV approach in our characterization of cortical FFRs. PLV is an amplitude-independent metric of response synchrony and thus has the advantage of more accurate separation of phase-locked response components from non-phase-locked activity. Also, PLVs are dimensionless units; this facilitates comparison across subjects. A potential weakness of this approach also stems from the fact that it is amplitude independent. As such, it may be too sensitive in picking up far-field activity, produc-

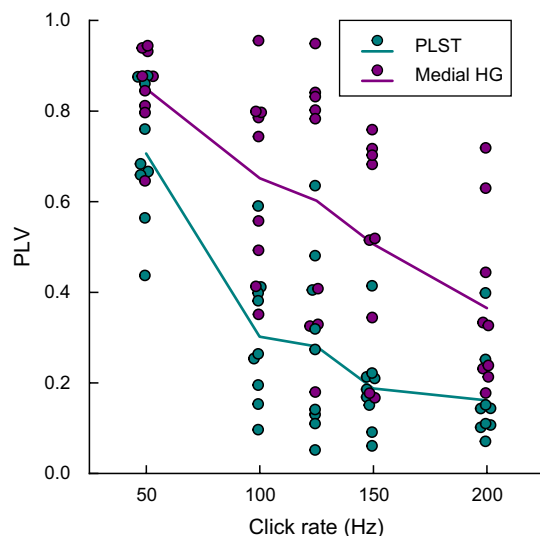


Fig. 8. Phase locking in medial HG and PLST. Summary of data from 9 subjects (L145, L162, L178, R149, R152, R153, R154, R180, and R186). PLVs are plotted as functions of click rate for sites within PLST and medial HG (teal and purple circles, respectively). Data from 1 medial HG and 1 PLST site that exhibited the highest PLVs at 50 Hz in each subject are shown. Purple and teal lines represent across-subject mean PLVs for medial HG and PLST sites, respectively. A small amount of variability was added to the abscissa values to make individual data points more visible.

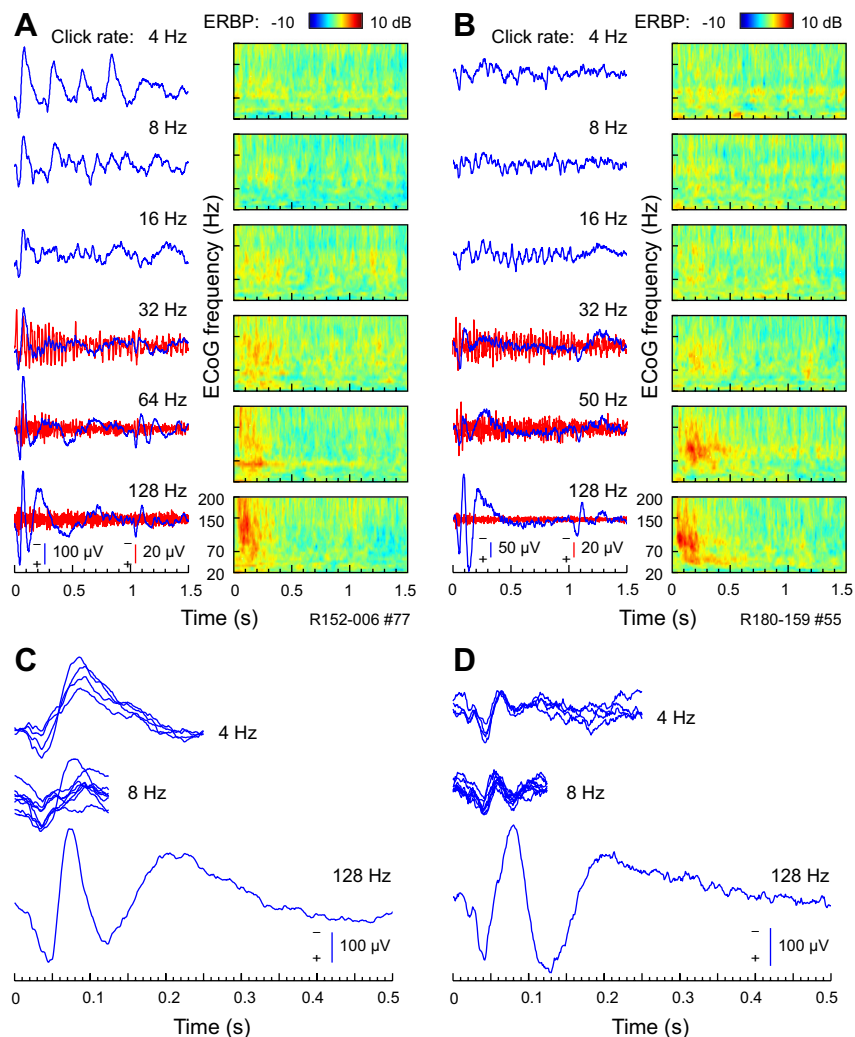


Fig. 9. PLST responses to 1-s click trains. *A* and *B*: all-pass (1.6–500 Hz) and high-pass (cut-off 1 octave below driving frequency) AEP waveforms (blue and red traces, respectively) and ERBP (color plots), elicited by click trains of rates between 4 and 128 Hz (*top to bottom*). Exemplary data from 2 representative right-hemisphere sites in 2 different subjects (R152 and R180, *A* and *B*, respectively). At a relatively low rate of 4 Hz, each click in the train evoked a distinct AEP complex (*top plots* in *A* and *B*). *C* and *D*: AEP waveforms recorded in response to 4- and 8-Hz click trains are replotted by fragmenting and superimposing the portions of the AEP waveform that were recorded between consecutive clicks in the click train. The 1st 500 ms of the AEP waveforms elicited by 128-Hz click trains is plotted below.

ing PLVs of spurious significance, and thus yielding false-positive results.

We attempted to minimize contribution of possible common sources by applying a spline Laplacian transform to the data. This procedure yields a noticeable increase in the spatial specificity of the recordings compared with unprocessed data [see Reale et al. (2007), for examples]. Sharp gradients in response magnitude between adjacent (5-mm apart) recording sites can be observed in Figs. 1 and 2. Finally, relatively fast ECoG components, including those in the high gamma frequency band and FFRs to comparable stimulus-driving frequencies, are recorded in close spatial proximity to their cortical sources and thus are highly localized (Frien et al. 2000; Liu and Newsome 2006).

Phase-locking analysis implemented in this study provides evidence for a high capacity of human non-primary of PLST for explicit temporal representation of periodicity. This raises a concern about possible far-field, volume-conducted sources of phase-locked activity recorded with subdural electrodes, originating, for example, from A1 or auditory brain stem nuclei. A clear difference in response morphology and upper limit of phase locking between recordings from PLST and medial HG makes a significant contribution of activity from the core auditory cortex to PLST recordings unlikely (see Fig. 7).

Furthermore, if FFRs recorded with electrodes placed over the lateral STG were volume conducted from the core auditory cortex, one might expect to obtain significant PLVs, mainly from sites located immediately adjacent to the Sylvian fissure. As can be observed from Figs. 3 and 4, this was not the case in our study.

Upper limits of phase locking that we obtained can be attributed to the abrupt onset of the clicks that we used and hence, stronger temporal locking compared with a more gradual ramping up of each cycle of the SAM signal (Heil 2003). Core neurons are as remarkably precise as auditory nerve fibers in their firing to an acoustic transient (Heil and Irvine 1997), which is a prerequisite in supporting a temporal representation of phonetically important speech components (Heil 2003; Heil and Irvine 1997; Phillips 1998; Phillips and Farmer 1990; Phillips and Hall 1990). Underlying this precision is a delicate balance of excitation and inhibition at the thalamocortical synapse (Tan et al. 2004; Wehr and Zador 2003).

The FFR reflects cortical activity that is phase locked to stimulus periodicity. It may be considered the simplest isomorphic form of temporal sound feature representation on the cortical level. The presence of FFRs to relatively fast (>30 Hz; i.e., above the lower limit of pitch) periodic stimuli raises questions concerning the functional use of such isomorphic

representations within the non-core auditory cortex. Several lines of evidence suggest that integrity of the A1 is required for processing such segmental components of speech, which exhibit temporal variations in the millisecond-to-tens-of-milliseconds range (Phillips and Farmer 1990), and the same may be said for area PLST. Phase-locked activity up to several tens of hertz may facilitate interneuronal communication, engaging large-scale networks involved in perception, and may play a critical role in multisensory interactions by, for example, synchronizing auditory and visual inputs (Doesburg et al. 2008; Hipp et al. 2011; Senkowski et al. 2005). Furthermore, animal studies demonstrate a relationship between behavioral training and phase-locked responses in the A1 (Bao et al. 2004; Schnupp et al. 2006), suggesting that preservation of the stimulus timing at the cortical level may also be beneficial for perception of behaviorally relevant sounds. These hypotheses can be tested in future studies that use active-listening tasks to investigate the relationship between the subject's perception of temporally dynamic stimuli and strength of phase-locked cortical responses.

High gamma response. Although phase locking to click trains generally decreased in strength with click rate beyond 50 Hz, auditory cortex within PLST maintained a representation of the stimuli by increases in high gamma power at higher stimulus rates. ERBP typically increased with stimulus repetition rate, at least up to ~150–200 Hz. This may be interpreted as a neural population-level correlate of a rate code for sound periodicity (e.g., Wang et al. 2008). Higher rates, above those for which phase locking is reliably exhibited, may be encoded as discharge rate, as suggested by Wang (2007). We observed also that the spatial distribution of non-phase-locked gamma activity within PLST changed with click rate. This finding suggests that for stimulus rates close to or beyond the limits of cortical-phase locking, information about stimulus rate may be represented in a more complex form by the spatial distribution of cortical activation.

Finally, although maps of the FFR and high gamma ERBP overlapped, their respective areas of maximal activity were not typically coextensive, particularly at higher click rates (see Fig. 6). This would suggest that within this overlapping auditory domain on posterolateral STG, the neural circuits underlying these two stimulus representations are, at least to some degree, segregated. Whereas this spatial disconnect was seen to be more pronounced in the left hemisphere compared with the right hemisphere, conclusions regarding laterality of the disconnect are tempered by the fact that it was not possible to record simultaneously from the two hemispheres in the same subject.

Comparison with core auditory cortex. The power of our experimental approach is that cortical activity may be recorded simultaneously from multiple auditory fields. We were, therefore, able to directly compare for each subject activity evoked by click trains in PLST with that evoked in presumed core and adjacent non-core areas of HG. Here, we compare specifically the capacity of these areas to phase lock to the click-train stimulus. These and other details of responses of HG core and belt cortex to click-train stimulation have been presented previously (Brugge et al. 2008, 2009). Simultaneous recordings in these areas were distinguishable by their AEP waveform complexes, ERBP and FFR. Robust phase locking to clicks was confined to HG core and PLST areas. This is despite the fact

that the auditory HG core receives its major afferent input from the ventral medial geniculate body, whereas PLST, if similar to connections in nonhuman primates, most likely receives a convergent input from the core and from extralemniscal-ascending auditory pathways, including medial geniculate complex and pulvinar (de la Mothe et al. 2012).

Responses to click trains recorded from PLST exhibited a certain degree of similarity, with activity measured in the core auditory cortex within posteromedial HG. In both regions, three basic response features—AEP waveform complexes, FFR, and ERBP—could be identified. Qualitative changes in response properties that parallel perceptual classes of repetitive stimuli were found both in the auditory core and PLST (cf. Brugge et al. 2009; Nourski and Brugge 2011). Specific features include changes in the shape of AEP waveforms elicited by successive clicks at and above 8 Hz, corresponding to perceptual blending of clicks into a unified, flutter-like percept, and the emergence of distinct AEP on and off responses and high gamma ERBP at stimulus rates above ~30 Hz, thus corresponding to the lower limit of pitch in human listeners (Krumbholz et al. 2000).

Differences between the core auditory cortex and PLST include overall morphology of the AEP complexes [see also Brugge et al. (2008)]. The strength of phase locking within PLST for a nonprimary cortical region is consistently lower than that in the core [see also Brugge et al. (2009) and Nourski and Brugge (2011)]. In addition, whereas the timing of each click was typically represented by a burst in ERBP for relatively low-rate stimuli (<32 Hz) within the core auditory cortex, no bursts or modulation of high gamma ERBP at low stimulus rates were observed in recordings made from PLST. Thus the mechanisms that sustain phase locking of the AEP in both core and PLST are not retained in the high gamma range of activity in PLST. Overall, the presence of robust responses to click trains in PLST and its high capacity for explicit temporal representation of periodicity suggest that this cortex, whereas functionally distinct from the auditory core, is relatively close to it within the hierarchy of auditory cortical fields. Nevertheless, as we and others have suggested previously, there is still no consensus on the number of areas present or their arrangement in human auditory cortex, including this area of the posterior STG (Brugge et al. 2008; Hackett 2011). Further studies using more complex stimuli will further investigate the functional identity of the auditory cortex of PLST.

ACKNOWLEDGMENTS

We thank Haiming Chen and Rachel Gold for help with data collection and analysis.

GRANTS

Support for this work was provided by the National Institute on Deafness and Other Communication Disorders (Grant Number R01-DC04290), National Center for Research Resources (Grant Number UL1RR024979), National Center for Advancing Translational Sciences, Hearing Health Foundation (Collette Ramsey Baker Award), and Hoover Fund.

DISCLOSURES

No conflicts of interest, financial or otherwise, are declared by the authors.

AUTHOR CONTRIBUTIONS

Author contributions: K.V.N., J.F.B., and M.A.H. conception and design of research; K.V.N., R.A.R., H.O., and H.K. performed experiments; K.V.N., R.A.R., C.K.K., H.O., and R.L.J. analyzed data; K.V.N., J.F.B., R.A.R., and C.K.K. interpreted results of experiments; K.V.N. and J.F.B. prepared figures; K.V.N., J.F.B., and R.A.R. drafted manuscript; K.V.N., J.F.B., R.A.R., C.K.K., H.O., H.K., R.L.J., and M.A.H. edited and revised manuscript; K.V.N., J.F.B., R.A.R., C.K.K., H.O., H.K., R.L.J., and M.A.H. approved final version of manuscript.

REFERENCES

- Bao S, Chang EF, Woods J, Merzenich MM.** Temporal plasticity in the primary auditory cortex induced by operant perceptual learning. *Nat Neurosci* 7: 974–981, 2004.
- Benjamini Y, Drai D, Elmer G, Kafkari N, Golani I.** Controlling the false discovery rate in behavior genetics research. *Behav Brain Res* 125: 279–284, 2001.
- Benjamini Y, Hochberg Y.** Controlling the false discovery rate: a practical and powerful approach to multiple testing. *J Royal Stat Soc B Methodol* 57: 289–300, 1995.
- Brugge JF, Nourski KV, Oya H, Reale RA, Kawasaki H, Steinschneider M, Howard MA III.** Coding of repetitive transients by auditory cortex of Heschl's gyrus of human. *J Neurophysiol* 102: 2358–2374, 2009.
- Brugge JF, Volkov IO, Garell PC, Reale RA, Howard MA III.** Functional connections between auditory cortex on Heschl's gyrus and on the lateral superior temporal gyrus in humans. *J Neurophysiol* 90: 3750–3763, 2003.
- Brugge JF, Volkov IO, Oya H, Kawasaki H, Reale RA, Fenoy A, Steinschneider M, Howard MA III.** Functional localization of auditory cortical fields of human: click-train stimulation. *Hear Res* 238: 12–24, 2008.
- Brugge JF, Volkov IO, Reale RA, Garell PC, Kawasaki H, Oya H, Li Q, Howard MA III.** The posterolateral superior temporal auditory field in humans: functional organization and connectivity. In: *Auditory Cortex. A Synthesis of Human and Animal Research*, edited by Konig R, Heil P, Budinger E, and Scheich H. Mahwah, NJ: Erlbaum, 2005, p. 145–162.
- Buszaki G.** *Rhythms of the Brain*. New York: Oxford University Press, 2006.
- Chavez M, Besserve M, Adam C, Martinerie J.** Towards a proper estimation of phase synchronization from time series. *J Neurosci Methods* 154: 149–160, 2006.
- Chevillet M, Riesenhuber M, Rauschecker JP.** Functional correlates of the anterolateral processing hierarchy in human auditory cortex. *J Neurosci* 31: 9345–9352, 2011.
- Chiry O, Tardif E, Magistretti PJ, Clarke S.** Patterns of calcium-binding proteins support parallel and hierarchical organization of human auditory areas. *Eur J Neurosci* 17: 397–410, 2003.
- Crone NE, Boatman D, Gordon B, Hao L.** Induced electrocorticographic gamma activity during auditory perception. *Clin Neurophysiol* 112: 565–582, 2001.
- de la Mothe LA, Blumell S, Kajikawa Y, Hackett TA.** Thalamic connections of auditory cortex in marmoset monkeys: lateral belt and parabelt regions. *Anat Rec (Hoboken)* 295: 822–836, 2012.
- Doesburg SM, Emberson LL, Rahi A, Cameron D, Ward LM.** Asynchrony from synchrony: long-range gamma-band neural synchrony accompanies perception of audiovisual speech asynchrony. *Exp Brain Res* 185: 11–20, 2008.
- Edwards E, Soltani M, Kim W, Dalal SS, Nagarajan SS, Berger MS, Knight RT.** Comparison of time-frequency responses and the event-related potential to auditory speech stimuli in human cortex. *J Neurophysiol* 102: 377–386, 2009.
- Frien A, Eckhorn R, Bauer R, Woelbern T, Gabriel A.** Fast oscillations display sharper orientation tuning than slower components of the same recordings in striate cortex of the awake monkey. *Eur J Neurosci* 12: 1453–1465, 2000.
- Fullerton BC, Pandya DN.** Architectonic analysis of the auditory-related areas of the superior temporal region in human brain. *J Comp Neurol* 504: 470–498, 2007.
- Giraud AL, Lorenzi C, Ashburner J, Wable J, Johnsrude I, Frackowiak R, Kleinschmidt A.** Representation of the temporal envelope of sounds in the human brain. *J Neurophysiol* 84: 1588–1598, 2000.
- Gourévitch B, Le Bouquin-Jeannès R, Faucon G, Liégeois-Chauvel C.** Temporal envelope processing in the human auditory cortex: response and interconnections of auditory cortical areas. *Hear Res* 237: 1–18, 2008.
- Hackett TA.** Anatomical organization of the auditory cortex. *J Am Acad Audiol* 19: 774–779, 2008.
- Hackett TA.** Information flow in the auditory cortical network. *Hear Res* 271: 133–146, 2011.
- Hackett TA.** Organization and correspondence of the auditory cortex of humans and nonhuman primates. In: *Evolution of the Nervous System*, edited by Kaas JH. Oxford, UK: Elsevier, 2007, p. 109–119.
- Hackett TA.** The comparative anatomy of the primate auditory cortex. In: *Primate Audition: Ethology and Neurobiology*, edited by Ghazanfar AA. Boca Raton, FL: CRC, 2003, p. 199–219.
- Hackett TA, Preuss TM, Kaas JH.** Architectonic identification of the core region in auditory cortex of macaques, chimpanzees, and humans. *J Comp Neurol* 441: 197–222, 2001.
- Harms MP, Melcher JR.** Sound repetition rate in the human auditory pathway: representations in the waveshape and amplitude of fMRI activation. *J Neurophysiol* 88: 1433–1450, 2002.
- Heil P.** Coding of temporal onset envelope in the auditory system. *Speech Commun* 41: 123–134, 2003.
- Heil P, Irvine DR.** First-spike timing of auditory-nerve fibers and comparison with auditory cortex. *J Neurophysiol* 78: 2458–2454, 1997.
- Hipp JF, Engel AK, Siegel M.** Oscillatory synchronization in large-scale cortical networks predicts perception. *Neuron* 69: 387–396, 2011.
- Howard MA, Nourski KV, Brugge JF.** Invasive research methods. In: *Human Auditory Cortex*, edited by Poeppel D, Overath T, Popper AN, and Fay RR. New York: Springer Science + Business Media, 2012, p. 39–67.
- Howard MA, Volkov IO, Abbas PJ, Damasio H, Ollendieck MC, Granner MA.** A chronic microelectrode investigation of the tonotopic organization of human auditory cortex. *Brain Res* 724: 260–264, 1996.
- Howard MA, Volkov IO, Mirsky R, Garell PC, Noh MD, Granner M, Damasio H, Steinschneider M, Reale RA, Hind JE, Brugge JF.** Auditory cortex on the posterior superior temporal gyrus of human cerebral cortex. *J Comp Neurol* 416: 76–92, 2000.
- Hutslers JJ, Gazzaniga MS.** Acetylcholinesterase staining in human auditory and language cortices: regional variation of structural features. *Cereb Cortex* 6: 260–270, 1996.
- Imaizumi K, Priebe NJ, Sharpee TO, Cheung SW, Schreiner CE.** Encoding of temporal information by timing, rate, and place in cat auditory cortex. *PLoS One* 5: e11531, 2010.
- Jenkinson M, Bannister P, Brady J, Smith S.** Improved optimization for the robust and accurate linear registration and motion correction of brain images. *Neuroimage* 17: 825–841, 2002.
- Jervis BW, Nichols MJ, Johnson TE, Allen E, Hudson NR.** A fundamental investigation of the composition of auditory evoked potentials. *IEEE Trans Biomed Eng* 30: 43–50, 1983.
- Joris PX, Schreiner CE, Rees A.** Neural processing of amplitude-modulated sounds. *Physiol Rev* 84: 541–577, 2004.
- Kaas JH, Hackett TA.** Subdivisions and connections of auditory cortex in primates: a working model. In: *Auditory Cortex. A Synthesis of Human and Animal Research*, edited by Konig R, Heil P, Budinger E, and Scheich H. Mahwah, NJ: Erlbaum, 2005, p. 7–26.
- Krumholz K, Patterson RD, Pressnitzer D.** The lower limit of pitch as determined by rate discrimination. *J Acoust Soc Am* 108: 1170–1180, 2000.
- Kuwada S, Batra R, Maher VL.** Scalp potentials of normal and hearing-impaired subjects in response to sinusoidally amplitude-modulated tones. *Hear Res* 21: 179–192, 1986.
- Lachaux JP, Rodriguez E, Martinerie J, Varela FJ.** Measuring phase synchrony in brain signals. *Hum Brain Mapp* 8: 194–208, 1999.
- Langner G.** Periodicity coding in the auditory system. *Hear Res* 60: 115–142, 1992.
- Law SK, Nunez PL, Wijesinghe RS.** High-resolution EEG using spline generated surface Laplacians on spherical and ellipsoidal surfaces. *IEEE Trans Biomed Eng* 40: 145–153, 1993.
- Liang L, Lu T, Wang X.** Neural representations of sinusoidal amplitude and frequency modulations in the primary auditory cortex of awake primates. *J Neurophysiol* 87: 2237–2261, 2002.
- Liégeois-Chauvel C, Lorenzi C, Trébuchon A, Régis J, Chauvel P.** Temporal envelope processing in the left and right auditory cortices. *Cereb Cortex* 14: 731–740, 2004.
- Liegeois-Chauvel C, Musolino A, Chauvel P.** Localization of the primary auditory area in man. *Brain* 114: 139–151, 1991.
- Liu J, Newsome WT.** Local field potential in cortical area MT: stimulus tuning and behavioral correlations. *J Neurosci* 26: 7779–7790, 2006.
- Lu T, Liang L, Wang X.** Temporal and rate representations of time-varying signals in the auditory cortex of awake primates. *Nat Neurosci* 4: 1131–1138, 2001.

- Mardia KV, Jupp PE.** *Directional Statistics*. Hoboken, NJ: John Wiley & Sons, 2000.
- Mukamel R, Fried I.** Human intracranial recordings and cognitive neuroscience. *Annu Rev Psychol* 63: 511–537, 2012.
- Nakahara H, Yamada S, Mizutani T, Murayama S.** Identification of the primary auditory field in archival human brain tissue via immunocytochemistry of parvalbumin. *Neurosci Lett* 286: 29–32, 2000.
- Nir Y, Fisch L, Mukamel R, Gelbard-Sagiv H, Arieli A, Fried I, Malach R.** Coupling between neuronal firing rate, gamma LFP, and BOLD fMRI is related to interneuronal correlations. *Curr Biol* 17: 1275–1285, 2007.
- Nourski K, Brugge J, Reale R, Kawasaki H, Oya H, Kovach C, Howard M.** Responses to repetitive transients within human lateral superior temporal gyrus: an intracranial electrophysiology study. Association for Research in Otolaryngology 2011 MidWinter Meeting, February 19–23, 2011, Baltimore, MD. *Assoc Res Otolaryngol Abstr*, 2011.
- Nourski KV, Brugge JF.** Representation of temporal sound features in the human auditory cortex. *Rev Neurosci* 22: 187–203, 2011.
- Nunez P.** *Electric Fields of the Brain*. New York: Oxford University Press, 1981.
- Nunez PL, Pilgreen KL.** The Spline-Laplacian in clinical neurophysiology: a method to improve EEG spatial resolution. *J Clin Neurophysiol* 8: 397–413, 1991.
- Oya H, Kawasaki H, Howard MA III, Adolphs R.** Electrophysiological responses in the human amygdala discriminate emotion categories of complex visual stimuli. *J Neurosci* 22: 9502–9512, 2002.
- Pawitan Y.** In *All Likelihood: Statistical Modeling and Inference Using Likelihood*. Oxford, UK: Clarendon, 2001.
- Perrin F, Pernier J, Bertrand O, Giard MH, Echallier JF.** Mapping of scalp potentials by surface spline interpolation. *Electroencephalogr Clin Neurophysiol* 66: 75–81, 1987.
- Phillips DP.** Sensory representations, the auditory cortex, and speech perception. *Semin Hear* 19: 319–331, 1998.
- Phillips DP, Farmer ME.** Acquired word deafness, and the temporal grain of sound representation in the primary auditory cortex. *Behav Brain Res* 40: 85–94, 1990.
- Phillips DP, Hall SE.** Response timing constraints on the cortical representation of sound time structure. *J Acoust Soc Am* 88: 1403–1411, 1990.
- Rauschecker JP, Scott SK.** Maps and streams in the auditory cortex: nonhuman primates illuminate human speech processing. *Nat Neurosci* 12: 718–724, 2009.
- Reale RA, Calvert GA, Thesen T, Jenison RL, Kawasaki H, Oya H, Howard MA, Brugge JF.** Auditory-visual processing represented in the human superior temporal gyrus. *Neuroscience* 145: 162–184, 2007.
- Reddy CG, Dahdaleh NS, Albert G, Chen F, Hansen D, Nourski K, Kawasaki H, Oya H, Howard MA III.** A method for placing Heschl gyrus depth electrodes. *J Neurosurg* 112: 1301–1307, 2010.
- Rees A, Green GG, Kay RH.** Steady-state evoked responses to sinusoidally amplitude-modulated sounds recorded in man. *Hear Res* 23: 123–133, 1986.
- Rivier F, Clarke S.** Cytochrome oxidase, acetylcholinesterase, and NADPH-diaphorase staining in human supratemporal and insular cortex: evidence for multiple auditory areas. *Neuroimage* 6: 288–304, 1997.
- Ross B, Borgmann C, Draganova R, Roberts LE, Pantev C.** A high-precision magnetoencephalographic study of human auditory steady-state responses to amplitude-modulated tones. *J Acoust Soc Am* 108: 679–681, 2000.
- Schnupp JW, Hall TM, Kokelaar RF, Ahmed B.** Plasticity of temporal pattern codes for vocalization stimuli in primary auditory cortex. *J Neurosci* 26: 4785–4795, 2006.
- Senkowski D, Talsma D, Herrmann CS, Woldorff MG.** Multisensory processing and oscillatory gamma responses: effects of spatial selective attention. *Exp Brain Res* 166: 411–426, 2005.
- Steinschneider M, Nourski KV, Kawasaki H, Oya H, Brugge JF, Howard MA III.** Intracranial study of speech-elicited activity on the human posterolateral superior temporal gyrus. *Cereb Cortex* 21: 2332–2347, 2011.
- Steinschneider M, Reser DH, Fishman YI, Schroeder CE, Arezzo JC.** Click train encoding in primary auditory cortex of the awake monkey: evidence for two mechanisms subserving pitch perception. *J Acoust Soc Am* 104: 2935–2955, 1998.
- Steinschneider M, Schroeder CE, Arezzo JC, Vaughan HG Jr.** Speech-evoked activity in primary auditory cortex: effects of voice onset time. *Electroencephalogr Clin Neurophysiol* 92: 30–43, 1994.
- Steinschneider M, Tenke CE, Schroeder CE, Javitt DC, Simpson GV, Arezzo JC, Vaughan HG Jr.** Cellular generators of the cortical auditory evoked potential initial component. *Electroencephalogr Clin Neurophysiol* 84: 196–200, 1992.
- Sweet RA, Dorph-Petersen KA, Lewis DA.** Mapping auditory core, lateral belt, and parabelt cortices in the human superior temporal gyrus. *J Comp Neurol* 491: 270–289, 2005.
- Tan AY, Zhang LI, Merzenich MM, Schreiner CE.** Tone-evoked excitatory and inhibitory synaptic conductances of primary auditory cortex neurons. *J Neurophysiol* 92: 630–643, 2004.
- Vaughan HG Jr.** The relationship of brain activity to scalp recordings of event-related potentials. In: *Average Evoked Potentials. Methods, Results and Evaluations*, edited by Donchin E and Lindsley DB. Washington, DC: National Aeronautics and Space Administration, 1969, p. 45–75.
- Vaughan HG Jr, Arezzo JC.** The neural basis of event-related potentials. In: *Human Event-Related Potentials*, edited by Picton TW. Amsterdam: Elsevier, 1988, vol. 3, p. 45–96.
- Wallace MN, Johnston PW, Palmer AR.** Histochemical identification of cortical areas in the auditory region of the human brain. *Exp Brain Res* 143: 499–508, 2002.
- Wang X.** Neural coding strategies in auditory cortex. *Hear Res* 229: 81–93, 2007.
- Wang X, Lu T, Bendor D, Bartlett E.** Neural coding of temporal information in auditory thalamus and cortex. *Neuroscience* 157: 484–494, 2008.
- Wang X, Lu T, Liang L.** Cortical processing of temporal modulations. *Speech Commun* 41: 107–121, 2003.
- Wehr M, Zador AM.** Balanced inhibition underlies tuning and sharpens spike timing in auditory cortex. *Nature* 426: 442–446, 2003.
- Whittingstall K, Logothetis NK.** Frequency-band coupling in surface EEG reflects spiking activity in monkey visual cortex. *Neuron* 64: 281–289, 2009.